



**HAL**  
open science

**Synthesis, crystal structure and magnetic behavior of a  
new calcium magnesium and iron orthophosphate  
 $\text{Ca}_2\text{MgFe}_2(\text{PO}_4)_4$**

Ahmed Ould Saleck, C. Mercier, C. Follet, Olivier Mentré, Abderrazzak  
Assani, M. Saadi, L. El Ammari

► **To cite this version:**

Ahmed Ould Saleck, C. Mercier, C. Follet, Olivier Mentré, Abderrazzak Assani, et al.. Synthesis, crystal structure and magnetic behavior of a new calcium magnesium and iron orthophosphate  $\text{Ca}_2\text{MgFe}_2(\text{PO}_4)_4$ . Journal of Solid State Chemistry, 2020, 292, pp.121715. 10.1016/j.jssc.2020.121715 . hal-03094584

**HAL Id: hal-03094584**

**<https://hal.science/hal-03094584>**

Submitted on 28 Nov 2022

**HAL** is a multi-disciplinary open access archive for the deposit and dissemination of scientific research documents, whether they are published or not. The documents may come from teaching and research institutions in France or abroad, or from public or private research centers.

L'archive ouverte pluridisciplinaire **HAL**, est destinée au dépôt et à la diffusion de documents scientifiques de niveau recherche, publiés ou non, émanant des établissements d'enseignement et de recherche français ou étrangers, des laboratoires publics ou privés.

# Synthesis, crystal structure and magnetic behavior of a new calcium magnesium and iron orthophosphate $\text{Ca}_2\text{MgFe}_2(\text{PO}_4)_4$

A. Ould Saleck<sup>a,b</sup>, C. Mercier<sup>a\*</sup>, C. Follet<sup>a</sup>, O. Mentré<sup>c</sup>, A. Assani<sup>b</sup>, M. Saadi<sup>b</sup>, and L. El Ammari<sup>b</sup>

<sup>a</sup>Laboratoire des Matériaux Céramiques et Procédés Associés – LMCPA, Université Polytechnique Hauts-de-France, F-59313 Valenciennes, France.

<sup>b</sup>Laboratoire de Chimie Appliquée des Matériaux, Centre des Sciences des Matériaux, Faculty of Science, Mohammed V University in Rabat, Avenue Ibn Batouta, BP 1014, Rabat, Morocco.

<sup>c</sup>Unité de Catalyse et Chimie du Solide – UCCS, Université Lille 1, F-59000 Lille, France.

\*corresponding author

## ABSTRACT

The structure of the new calcium magnesium iron orthophosphate,  $\text{Ca}_2\text{MgFe}_2(\text{PO}_4)_4$  was determined from single crystal X-ray diffraction data. It crystallizes in the orthorhombic system, space group  $Pbca$ , with all atoms in general positions among which two sites are disordered. The crystal structure of this phosphate is build up from  $\text{PO}_4$  tetrahedra linked to  $\text{FeO}_6$  octahedra and to  $(\text{Fe/Mg})\text{O}_5$  polyhedra via common vertices. In fact, each of the two mixed sites  $(\text{Fe/Mg})$  is surrounded by five oxygen atoms which form either a pyramid with a square base or a bi-pyramid with a triangular base. The interconnection of these polyhedra leads to a three-dimensional structure delimiting cavities where  $\text{Ca}^{2+}$  cations are localized. The powder of this compound was successfully obtained by solid state reaction and its X-ray diffraction diagram was refined by pattern matching method. The magnetic measurements show multiple transition assigned to frustrated triangles locally present in AFM magnetic layered units.

## Keywords :

### 1. Introduction

The orthophosphate compounds have received a great attention owing to its structural richness. All structures of those compounds are based on the connection of  $\text{PO}_4$  tetrahedral groups with  $\text{MO}_n$  polyhedra (M generally represents transition and /or alkaline earth metals). According to its structural type and the nature of the metal cations, many physical and chemical properties can be observed for these class of materials such as: electrochemical [1–

5], magnetic [6–8] and catalytic properties [9–11]. Moreover, It is well known that the orthophosphate compounds doped by the rare-earth elements exhibit a very interesting luminescence properties [12–15].

In this context, our focus of interest is axed on the tetra-orthophosphate based materials. On the basis of our bibliographic analysis, those phosphates can be represented with the general formula,  $M_3M'_3(PO_4)_4$ ,  $A_2(M/M')_5(PO_4)_4$  or  $A_3M''_3(PO_4)_4$  (A, M/M' and M'' represent mono-, bi- and trivalent cations respectively). Accordingly, it has been found that the members of the  $M_3M'_3(PO_4)_4$  phosphates group,  $M_3Cu_3(PO_4)_4$  (M = Ca, Sr and Pb) and  $Ca_3Mg_3(PO_4)_4$ , crystallize in the monoclinic system with different space groups [16–19]. However, the tetra-orthophosphate  $A_2(M/M')_5(PO_4)_4$ , namely  $Na_2Cd_5(PO_4)_4$  [20],  $Na_2Ca_5(PO_4)_4$  [21],  $Na_2Mg_5(PO_4)_4$  [22],  $Na_2Zn_5(PO_4)_4$  [23],  $Li_2Cu_5(PO_4)_4$  [24] and  $Cs_2Zn_5(PO_4)_4$  [25], known till now, represent a structurally rich group since those phosphates adopt different crystal structure in triclinic, monoclinic, quadratic or hexagonal systems. Moreover, a great deal of interest has been accorded to the third tetra-orthophosphate group,  $K_3Cr_3(PO_4)_4$  [26],  $Na_3Fe_3(PO_4)_4$  [27] and  $Na_3V_3(PO_4)_4$  [28], which crystallize in the orthorhombic and monoclinic system respectively, owing to its interesting properties in the electrochemistry applications as positive electrodes for sodium batteries [27, 28]. Besides, it is worth to mention the rarely encountered tetra-phosphates: (i) the bi- and trivalent cations based tetra-phosphates  $Pb_3Fe_2(PO_4)_4$  [29] and  $Ba_3Bi_2(PO_4)_4$  [30] both adopt a monoclinic symmetry and (ii) the only tetra-orthophosphate  $NaCaFe_3(PO_4)_4$ , grouping mono-, di- and trivalent cations which crystallizes in the orthorhombic system [31].

In the present work, we aim to develop the synthesis, the crystal structure determination from single crystal x-ray diffraction data and magnetic properties of a new calcium, magnesium and iron phosphate, namely  $Ca_2MgFe_2(PO_4)_4$ .

## 2. Experimental

### 2.1. Synthesis

Both single crystal and powder of the title phosphate  $Ca_2MgFe_2(PO_4)_4$  were synthesized from stoichiometric mixtures of  $CaCO_3$  (Fisher Chemical 98%),  $MgO$  (Fisher Chemical 95%),  $Fe_2O_3$  (Fisher Chemical 99.99%) and  $NH_4H_2PO_4$  by the solid-state reaction. Two stoichiometric mixtures were progressively heated up in a platinum crucible at 300°C, 400°C, 500°C and 600°C. The first product was melted at 980°C and maintained at this temperature during 10 min before being slowly cooled to 300°C at a rate of 5°C/h. The final product

consisted of transparent single crystals of the title compound. While, the second mixture has undergone heat treatments up to 700 °C where it is kept for 6 days to obtain the  $\text{Ca}_2\text{MgFe}_2(\text{PO}_4)_4$  pure powder.

## 2.2. Experimental Techniques

The  $\text{Ca}_2\text{MgFe}_2(\text{PO}_4)_4$  structure was determined at room temperature by single crystal X-ray diffraction using a four-circles diffractometer Bruker X8 equipped with an Apex II CCD detector and graphite monochromator for Mo  $K\alpha$  radiation,  $\lambda = 0.71073 \text{ \AA}$ . The software APEX2 was used for data collection and SAINT for cell refinement and data reduction. Absorption corrections were made using the SADABS program [32] from equivalent reflections on the basis of multiscans. The crystal structure was solved using direct method and refined by SHELXT 2013 [33] and SHELXL 2013 [34] programs incorporated in the WinGX [35] program. For structural drawing, DIAMOND [36] was used. The X-ray diffraction diagram (XRD) of  $\text{Ca}_2\text{MgFe}_2(\text{PO}_4)_4$  powder was collected using Panalytical X'pert Pro diffractometer, with Bragg-Brentano geometry ( $\theta-2\theta$ ) and a X-ray tube with a copper anticathode ( $\lambda_{K\alpha 1} = 1.54056 \text{ \AA}$  ;  $\lambda_{K\alpha 2} = 1.54441 \text{ \AA}$ ). The diffraction pattern was recorded in  $2\theta = 10^\circ - 100^\circ$  angular range with a measurement step of  $0.02^\circ$  and a counting time of 30 s pro step. The  $\text{Ca}_2\text{MgFe}_2(\text{PO}_4)_4$  powder XRD diagram was refined using pattern matching method with Jana 2006 program [37]. The Infrared spectrum of  $\text{Ca}_2\text{MgFe}_2(\text{PO}_4)_4$  was recorded between 400 and 4000  $\text{cm}^{-1}$  region using the JASCO FT/IR-4600 spectrometer. The spectrum measurement is made on pellet prepared from a mixture of 1% of  $\text{Ca}_2\text{MgFe}_2(\text{PO}_4)_4$  in KBr. The susceptibility versus temperature ( $H = 0.05$  and  $0.1 \text{ T}$ ) and magnetization versus field (at various temperatures) data have been collected on a polycrystalline sample between 1.8 K and 400 K until  $H = 9\text{T}$ , using a PPMS Dynacool (Quantum Design) system. Zero field cooled and Field Cooled routines have been employed for  $\chi(T)$ .

## 3. Results and discussion

### 3.1. Crystal structure determination

The crystal structure of  $\text{Ca}_2\text{MgFe}_2(\text{PO}_4)_4$  was determined from single crystal XRD data in the orthorhombic system with the  $Pbca$  space group and the unit cell parameters:  $a = 9.3357(7) \text{ \AA}$  ;  $b = 8.7340(6) \text{ \AA}$  and  $c = 29.422(2) \text{ \AA}$ . The Fe1, Fe2, Ca1, Ca2, Mg1 , P1, P2, P3 and P4 atoms are localized using the direct method by means of SHLEXS97 program [34]. After the refinement of those cationic positions, sixteen  $\text{O}^{2-}$  anions have been localized in a Fourier difference map and refined by the least square method. All these ions are in fully occupied

general positions (8c) of the Pbc<sub>a</sub> space group. However, the structure presents a disorder in two cationic sites. Indeed, the Fe<sub>2</sub> site is shared by 75% of iron and 25% of magnesium atoms, so called Fe<sub>2</sub>/Mg<sub>1</sub> site. The Mg<sub>1</sub> site is occupied by 75% of Mg and 25 % of Fe, so named Mg<sub>2</sub>/Fe<sub>3</sub> site. The validity of this model is corroborated by the final reliability factors obtained: R = 1.9 % and wR = 4.8 % with S = 1.08, in accordance with the crystallographic sites occupation and the charge neutrality. Crystal data and structure refinement parameters for Ca<sub>2</sub>MgFe<sub>2</sub>(PO<sub>4</sub>)<sub>4</sub> are summarized in Table 1. Atomic coordinates, occupancies and equivalent isotropic atomic displacement parameters, anisotropic displacement parameters for the studied phosphate are detailed in Table 2 and Table 3.

The Fe<sub>1</sub> atom is surrounded by six oxygen atoms to form an octahedral environment, Fe<sub>1</sub>O<sub>6</sub>, with the Fe<sub>1</sub>—O distances ranging from 1.973(1) Å to 2.079(1) Å as shown in Table 4. The Fe<sub>2</sub>/Mg<sub>1</sub> site presents a rectangular-based pyramidal geometry (Fe<sub>2</sub>/Mg<sub>1</sub>)O<sub>5</sub>. Significant Fe<sub>2</sub>/Mg<sub>1</sub>—O distances are summarized in Table 4. Five oxygen atoms surround the magnesium and iron atoms localized on the Mg<sub>2</sub>/Fe<sub>3</sub> site giving rise to triangular based bi-pyramidal geometry (Mg<sub>2</sub>/Fe<sub>3</sub>)O<sub>5</sub>. The Mg<sub>2</sub>/Fe<sub>3</sub>—O distances are extending from 1.991(1) Å to 2.050 (1) Å (Table 4) and the O<sub>1</sub> —Mg<sub>2</sub>/Fe<sub>3</sub>—O<sub>13</sub> angle is equal to 169.39(6) °.

Two of each polyhedron P<sub>2</sub>O<sub>4</sub>, P<sub>3</sub>O<sub>4</sub>, (Fe<sub>1</sub>)O<sub>6</sub> and (Mg<sub>2</sub>/Fe<sub>3</sub>)O<sub>5</sub> consecutively share vertices so as to construct the first kind of ring (Fig. 1a). Each ring is surrounded by eight other identical rings to form the first type of sheet in the (a, b) plane (Fig. 1b). A second kind of ring is made from the alternated connection of four P<sub>4</sub>O<sub>4</sub> and four rectangular-based pyramid (Fe<sub>2</sub>/Mg<sub>1</sub>)O<sub>5</sub> by means of corners (Fig. 1c). This latter ring is interconnected to eight other like rings to build a second type of sheet parallel to the plane (a, b) (Fig. 1d).

Two consecutive first kind layers are connected to each other with the P<sub>1</sub>O<sub>4</sub> tetrahedra so as to build double layers (Fig. 2a). Those double layers are connected by the second type of sheet (Fig. 2b) leading to a three-dimensional network delimiting cavities occupied by Ca<sup>2+</sup> cations (Fig. 3).

Based on our bibliographic analysis and to our knowledge, the present compound, Ca<sub>2</sub>MgFe<sub>2</sub>(PO<sub>4</sub>)<sub>4</sub>, shows an original structure which is similar to that of the only orthophosphate cited in the literature NaCaFe<sub>3</sub>(PO<sub>4</sub>)<sub>4</sub> [31]. However, the most important difference between the two structures lies in the disorder of the two cationic sites in the structure of the studied phosphate.

### 3.2. Powder X-ray diffraction analysis

The powder of the title phosphate was obtained after heat treatment at 700 °C during 6 days. Its corresponding XRD patterns profile was refined using “Le bail Method” [38] of Jana 2006

program [37]. The success of the refinement is attested by the good accordance between the observed ( $Y_{\text{obs}}$ ) and the calculated ( $Y_{\text{calc}}$ ) patterns as shown in Fig. 4. The final reliability factors obtained for this powder model are  $R_p = 1.59$ ,  $R_{wp} = 2.69$  and  $S = 1.81$ .

### 3.3. Infrared spectroscopy (IR)

Fig. 5 shows the infrared spectrum of  $\text{Ca}_2\text{MgFe}_2(\text{PO}_4)_4$ . The observed absorption bands at  $1148\text{ cm}^{-1}$ ,  $1084\text{ cm}^{-1}$  and  $1043\text{ cm}^{-1}$  can be assigned to  $\nu_3$  of P-O antisymmetric stretching mode. Besides, the band situated at  $1222\text{ cm}^{-1}$  can be likely assigned to the  $\nu_3$  mode of the shorter P-O. The band at  $980\text{ cm}^{-1}$  is associated to  $\nu_1$  of P-O symmetric stretching mode. The absorption bands at  $646\text{ cm}^{-1}$ ,  $603\text{ cm}^{-1}$ ,  $555\text{ cm}^{-1}$  and  $552\text{ cm}^{-1}$  can be assigned to the  $\nu_4$  symmetric modes. The peak around  $473$  is attributed to  $\nu_2$  mode. The presence of only isolated tetrahedra ( $\text{PO}_4^{3-}$ ) is confirmed by the absence of absorption bands between  $700\text{ cm}^{-1}$  and  $900\text{ cm}^{-1}$  which are the characteristic of the P-O-P angular deformation absorptions [24].

### 3.4. Magnetic properties

The magnetic properties of the title compounds are complicated by both the non-trivial iron connectivity in this dense phase, mostly mediated by  $\text{PO}_4$  bridges and by the mixed Fe/Mg occupancy within the  $\text{Fe}^{3+}$  ( $S = 5/2$ ,  $L = 0$ ) magnetic sublattice. For simplification, we assume here that the main bulk properties are driven by the fully occupied Fe1 and 75% occupied Fe2 sites. Fe3 being 25% occupied, we considered its influence as a local decoration of the main magnetic framework, subject to its influence, but enable to rule out the exchanges in a cooperative manner due to its high degree of dilution in the crystal. The ZFC and FC  $\chi(T)$  plots collected at  $\mu_0.H = 0.05\text{T}$  are given Fig. 6a. The 7K-400K region obeys a Curie weiss (CW) law:  $\chi = c/(T - \theta_{\text{CW}})$  and was fitted by  $\mu_{\text{eff}} = \sqrt{8C} = 5.83\ \mu_{\text{B}}/\text{Fe}^{3+}$  and  $\theta_{\text{CW}} = -38.5\text{ K}$ . The effective moment is in perfect agreement with the spin only value for  $\text{Fe}^{3+}$  ( $5.91\ \mu_{\text{B}}/\text{Fe}^{3+}$ ) which refutes any significant orbital contribution as expected for  $L = 0$  single ions. The negative CW temperature validate predominant validate antiferromagnetic exchanges, as expected by Goodenough-kanamori rules from any kind of  $\text{Fe}^{3+}\text{-O-Fe}^{3+}$  super-exchanges (SE) significantly different from  $90^\circ$  and for  $\text{Fe}^{3+}\text{-O-O-Fe}^{3+}$  super-super exchanges (SSE). As a matter of facts SSE paths predominate in  $\text{Ca}_2\text{MgFe}_2(\text{PO}_4)_4$  while only the Fe1(100%)-O-Fe3(25%) SE is achieved. One counts 8 and 7 SSE-neighbors around Fe1 and Fe2 respectively, leading to the average  $J/\text{K}_b$  Fe-Fe coupling of  $-1.75\text{K}$  using the mean field approximation  $\theta_{\text{CW}} = \sum_i z_i S(S+1) J_{i, \text{Fe-Fe}}/3\text{K}_b$  with  $z$  the average number of neighbors ( $=7.5$ ) and  $S = 5/2$ . This weak mean value does not take into consideration the distribution of

exchange values in the structure and one should empirically hierarchize them as discussed later, for a comprehensive interpretation. Their interaction is responsible for the complex low-T behavior resumed in Fig. 6b which shows: i) a magnetic ordering responsible for the sharp  $\chi(T)$  anomaly at  $T_N = 13.3$  K. ii) a second smeared transition at  $T_t = 5.7$  K with appearing at lower temperature of a net magnetic moment, as evidenced by the ZFC/FC divergence. This effect is marked in  $M(H)$  plots in the first  $0 \rightarrow 9T$  and second  $9T \rightarrow 0T$  branches below  $T_N$ .

- Here, during the field induced spin alignment (1<sup>st</sup> branch), a weak metamagnetic/spin flop transition is observed around  $H_{meta} \approx 2.7T$  at 2K as shown from the peak on  $dM/dH$ , see Fig. 6b, reminiscent of the closing of a low-field blocked spin configuration. This transition is prominent below  $T_t$ .

- Decreasing the field (2<sup>nd</sup> branch), this contribution is retained above a critical field  $H_C$ . We found  $H_C \approx 0.1T$  at  $T_N - 10K$ ,  $H_C \approx 0.056T$  at 5K, and  $H_C \approx 0.012T$  at 2K assorted with a remanent moment at zero field at the later temperature. This behavior is reminiscent of spin frustration that plausibly occurs as described below.

With the aim to give a plausible scenario, we should examine carefully the SSE's in competition. We checked that the strongest expected ones (i.e. according to the empirical criteria that they display the smallest dihedral/torsion Fe-O-O-Fe angles [39] to enhance the magnetic delocalization across  $p$  orbitals) are effective in the (a,c) layers dealing : strong  $J1_{(Fe1O-O-Fe1)}$ ,  $J2_{(Fe1-O-O-Fe2)}$  and weakest  $J3_{(Fe2-O-O-Fe2)}$  and  $J4_{(Fe2-O-O-Fe2)}$ , see Table 5. All together they define non-frustrated pseudo-hexagonal AFM layers, shown Fig. 7 where white and black Fe-sites denote *up* and *down* colinear spins with an arbitrary direction. We recall that the neglectable orbital contribution for  $Fe^{3+}$  ( $L = 0$ ) suggests anisotropic magnetic single ions, oriented by spin-lattice coupling (i.e. along specific crystallographic axes) rather than by local  $d$ -overlapping [40], such that a collinear spin-structure is presumed. Along the  $b$ -axis, the couplings between the layers also occur by SSE exchanges (Fe1-O-O-Fe1 and/or Fe2-O-O-Fe2), that we found in smaller extent in the crystal structure, according to the dense distribution of Fe ions within the (a,c) leaves. Fe3 (25% occ.) weakly perturbate the layers contribution below  $T_N$  but their contribution turns to significant on further cooling down to  $T_t$  or increasing the field until  $H_{meta}$ . In fact, the 25% of Fe3 are "locally" coupled to Fe1 by strong AFM super-exchanges  $J5$  with  $\angle Fe3-O-Fe1 = 104.3^\circ$ , but also coupled to Fe2 by significant SSE  $J6$  exchanges with  $\angle Fe3-O-O-Fe2 = 6.2^\circ$ . In Fine, it forms a statistic distribution (25%) of frustrated  $J2$ - $J5$ - $J6$  triangles, shown in red Fig.6. It is probable that the

Fe<sup>3+</sup> spin orientation is dominated by the SE J<sub>5</sub> below T<sub>N</sub> but should rapidly flop to a frustrated equilibrium position when all J<sub>s</sub> come in competition below T<sub>i</sub>. Such a situation validates an easy field-induced re-alignment, at the metamagnetic transition.

#### **4. Conclusion**

In this paper, we have reported a new calcium magnesium and iron orthophosphate, Ca<sub>2</sub>MgFe<sub>2</sub>(PO<sub>4</sub>)<sub>4</sub>, and it was characterized by single crystal, powder X-ray diffraction, infrared spectroscopy and magnetic susceptibility measurements. The structure of this compound shows an original structure type which is analogous to only one orthorhombic phosphate cited in the literature NaCaFe<sub>3</sub>(PO<sub>4</sub>)<sub>4</sub>. The major difference between the two structures is the presence of two disordered sites in the structure of Ca<sub>2</sub>MgFe<sub>2</sub>(PO<sub>4</sub>)<sub>4</sub>. The magnetic measurements show multiple transition assigned to frustrated triangles locally present in AFM magnetic layered units.

## References

- [1] K. Trad, Phosphates de fer de structures originales comme matériaux d'électrode positive pour batterie au lithium ou au sodium, Thèse de doctorat en cotutelle, Université Bordeaux 1/France et Faculté des Sciences de Monstir/Tunisie, 2010, HAL Id : tel-00563877, version 1.
- [2] J. Kim, H. Kim, I. Park, Y.-U. Park, J.-K. Yoo, K.-Y. Park, S. Lee, K. Kang, LiFePO<sub>4</sub> with an alluaudite crystal structure for lithium ion batteries, *Energy Environ. Sci.* 6 (2013) 830–834, <https://doi.org/10.1039/C3EE24393A>.
- [3] J. Kim, H. Kim, K.-Y. Park, Y.-U. Park, S. Lee, H.-S. Kwon, H.-I. Yoo, K. Kang, Alluaudite LiMnPO<sub>4</sub> : a new Mn-based positive electrode for Li rechargeable batteries, *J. Mater. Chem. A* 2 (2014) 8632–8636, <https://doi.org/10.1039/C4TA00955J>.
- [4] R. Essehli, I. Belharouak, H. Ben Yahia, K. Maher, A. Abouimrane, B. Orayech, S. Calder, X.L. Zhou, Z. Zhou, Y.-K. Sun, Alluaudite Na<sub>2</sub>Co<sub>2</sub>Fe(PO<sub>4</sub>)<sub>3</sub> as an electroactive material for sodium ion batteries, *Dalt. Trans.* 44 (2015) 7881–7886, <https://doi.org/10.1039/C5DT00971E>.
- [5] C. Masquelier, L. Croguennec, Polyanionic (Phosphates , Silicates , Sulfates) Frameworks as Electrode Materials for Rechargeable Li (or Na) Batteries, *Chem. Rev.* 113 (2013) 6552, <https://doi.org/10.1021/cr3001862>.
- [6] M. Riou-Cavellec, D. Riou, G. Férey, Magnetic iron phosphates with an open framework, *Inorganica Chim. Acta.* 291 (1999) 317–325, [https://doi.org/10.1016/S0020-1693\(99\)00132-2](https://doi.org/10.1016/S0020-1693(99)00132-2).
- [7] M. Hadouchi, A. Lahmar, M. El Marssi, Synthesis, Crystal Structure and Properties of a New Phosphate, Na<sub>2</sub>Co<sub>2</sub>Cr(PO<sub>4</sub>)<sub>3</sub>, *J. Inorg. Organomet. Polym. Mater.* (2018), <https://doi:10.1007/s10904-018-0956-y>.
- [8] D. Harbaoui, M.M.S. Sanad, C. Rossignol, E.K. Hlil, N. Amdouni, S. Obbade, Synthesis and Structural, Electrical, and Magnetic Properties of New Iron–Aluminum Alluaudite Phases β-Na<sub>2</sub>Ni<sub>2</sub>M(PO<sub>4</sub>)<sub>3</sub> (M = Fe and Al), *Inorg. Chem.* 56 (2017) 13051–13061, <https://doi.org/10.1021/acs.inorgchem.7b01880>.
- [9] J.E. Miller, M.M. Gonzales, L. Evans, A.G. Sault, C. Zhang, R. Rao, G. Whitwell, A. Maiti, D. King-smith, Oxidative dehydrogenation of ethane over iron phosphate catalysts, *Appl. Catal. A Gen.* 231 (2002) 281–292, [https://doi.org/10.1016/S0926-860X\(02\)00070-4](https://doi.org/10.1016/S0926-860X(02)00070-4).
- [10] J.B. Moffat, Phosphates as catalysts, *Catal. Rev. Sci. Eng.* 18 (1978) 199-258, <https://doi.org/10.1080/03602457808081868>.
- [11] M. Kacimi, M. Ziyad, F. Hatert, Structural features of AgCaCdMg<sub>2</sub>(PO<sub>4</sub>)<sub>3</sub> and AgCd<sub>2</sub>Mg<sub>2</sub>(PO<sub>4</sub>)<sub>3</sub>, two new compounds with the alluaudite-type structure, and their catalytic activity in butan-2-ol conversion, *Mater. Res. Bull.* 40 (2005) 682–693, <https://doi.org/10.1016/j.materresbull.2004.12.009>.
- [12] F. Yang, Y. Liu, X. Tian, G. Dong, Q. Yu, Journal of Solid State Chemistry Luminescence properties of phosphate phosphor Ba<sub>3</sub>Y(PO<sub>4</sub>)<sub>3</sub> : Sm<sup>3+</sup>, *J. Solid State Chem.* 225 (2015) 19–23, <https://doi:10.1016/j.jssc.2014.11.025>.
- [13] V. Pelova, K. Kynev, G. Gochev, Luminescence of alkali-earth phosphates activated

- with manganese and cerium, *J. Mater. Sci. Lett.* 14 (1995) 330–332, <https://doi.org/10.1007/BF00592141>.
- [14] A.K. Bedyal, A.K. Kunti, V. Kumar, H.C. Swart, Effects of cationic substitution on the luminescence behavior of Dy<sup>3+</sup> doped orthophosphate phosphor, *J. Alloys Compd.* 806 (2019) 1127–1137, <https://doi.org/10.1016/j.jallcom.2019.07.305>.
- [15] H. Donker, W.M.A. Smit, G. Blasse, On the Luminescence of Some Tin-Activated Alkaline-Earth Orthophosphates, *J. Electrochem. Soc.* 136 (1989) 3130–3135, <https://doi.org/10.1007/BF00592141>.
- [16] H. Effenberger, Sr<sub>3</sub>Cu<sub>3</sub>(PO<sub>4</sub>)<sub>4</sub>, Pb<sub>3</sub>Cu<sub>3</sub>(PO<sub>4</sub>)<sub>4</sub>, BaCu<sub>2</sub>(PO<sub>4</sub>)<sub>2</sub>·H<sub>2</sub>O, and Ba<sub>2</sub>Cu(PO<sub>4</sub>)<sub>2</sub>·H<sub>2</sub>O : Crystal Structures and Topological Relationships, *J. Solid State Chem.* 13 (1999) 6–13, <https://doi.org/10.1006/jssc.1998.7953>.
- [17] M. Drillon, M. Belaiche, P. Legoll, J. Aride, A. Boukhari, A. Moqine, 1D ferrimagnetism in copper(II) trimeric chains: Specific heat and magnetic behavior of A<sub>3</sub>Cu<sub>3</sub>(PO<sub>4</sub>)<sub>4</sub> with A = Ca, Sr, *J. Magn. Mater.* 128 (1993) 83–92, [https://doi.org/10.1016/0304-8853\(93\)90860-5](https://doi.org/10.1016/0304-8853(93)90860-5).
- [18] J.B. Anderson, E. Kostiner, F.A. Ruzsala, The Crystal Structure of Ca<sub>3</sub>Cu<sub>3</sub>(PO<sub>4</sub>)<sub>4</sub>, *J. Struct. Chem.* 34 (1981) 29–34, [https://doi.org/10.1016/0022-4596\(81\)90299-1](https://doi.org/10.1016/0022-4596(81)90299-1).
- [19] W. Wu, Z. Xia, Synthesis and color-tunable luminescence properties of Eu<sup>2+</sup> and Mn<sup>2+</sup>-activated Ca<sub>3</sub>Mg<sub>3</sub>(PO<sub>4</sub>)<sub>4</sub> phosphor for solid state lighting, *RSC Adv.* 3 (2013) 6051–6057, <https://doi.org/10.1039/C3RA40313K>.
- [20] T. Ben Hamed, A. Boukhris, B. Glorieux, M. Ben Amara, Synthesis , crystal structure and spectroscopic characterization of a new cadmium phosphate , Na<sub>2</sub>Cd<sub>5</sub>(PO<sub>4</sub>)<sub>4</sub>, *J. Mol. Struct.* 1199 (2020) 126963, <https://doi.org/10.1016/j.molstruc.2019.126963>.
- [21] G. Celotti, E. Landi, A misunderstood member of the nagelschmidite family unveiled : structure of Ca<sub>5</sub>Na<sub>2</sub>(PO<sub>4</sub>)<sub>4</sub> from X-ray powder diffraction data, *J. Eur. Ceram. Soc.* 23 (2003) 851–858, [https://doi.org/10.1016/S0955-2219\(02\)00211-X](https://doi.org/10.1016/S0955-2219(02)00211-X).
- [22] J. Yamakawa, T. Yamada, A. Kawahara, Un monophosphate de magnésium et de sodium, *Acta Crystallogr. Sect. C.* C50 (1994) 986–988, <https://doi.org/10.1107/S0108270193012004>.
- [23] L.N. Ji, H.W. Ma, J.B. Li, J.K. Liang, B.J. Sun, Y.H. Liu, J.Y. Zhang, G.H. Rao, A new structure type of phosphate : Crystal structure of Na<sub>2</sub>Zn<sub>5</sub>(PO<sub>4</sub>)<sub>4</sub>, *J. Solid State Chem.* 180 (2007) 2256–2261, <https://doi.org/10.1016/j.jssc.2007.05.027>.
- [24] L. Cui, S. Pan, J. Han, X. Dong, Z. Zhou, Synthesis , crystal structure and optical properties of Li<sub>2</sub>Cu<sub>5</sub>(PO<sub>4</sub>)<sub>4</sub>, *Solid State Sci.* 13 (2011) 1304–1308, <https://doi.org/10.1016/j.solidstatesciences.2011.03.026>.
- [25] F. Guo, J. Han, J. Cheng, Z. Yang, T. Abudouwufu, H. Yu, S. Pan, Cs<sub>2</sub>Zn<sub>5</sub>(PO<sub>4</sub>)<sub>4</sub> and Cs<sub>3</sub>La(PO<sub>4</sub>)<sub>2</sub>: Two Cs-Containing Phosphates with Three-Dimensional Frameworks, *Eur. J. Inorg. Chem.* 2019 (2019) 2462–2467, <https://doi.org/10.1002/ejic.201900241>.
- [26] S. Kouass, H. Boughzala, Tripotassium Trichrome (III) Tetraphosphate K<sub>3</sub>Cr<sub>3</sub>(PO<sub>4</sub>)<sub>4</sub>: Synthèse, Étude Structurale, Caractérisation et Conductivité Ionique, *Phosphorus Sulfur. Silicon Relat. Elem.* 181 (2006) 2641–2652, <https://doi.org/10.1080/10426500600862951>.

- [27] K. Trad, D. Carlier, L. Croguennec, A. Wattiaux, B. Lajmi, M. Ben Amara, C. Delmas, A Layered Iron(III) Phosphate Phase,  $\text{Na}_3\text{Fe}_3(\text{PO}_4)_4$  : Synthesis, Structure, and Electrochemical Properties as Positive Electrode in Sodium Batteries, *J. Phys. Chem. C*. 114 (2010) 10034–10044, <https://doi.org/10.1021/jp100751b>.
- [28] R. Liu, H. Liu, T. Sheng, S. Zheng, G. Zhong, G. Zheng, Z. Liang, G.F. Ortiz, W. Zhao, J. Mi, Y. Yang, Novel 3.9 V Layered  $\text{Na}_3\text{V}_3(\text{PO}_4)_4$  Cathode Material for Sodium Ion Batteries, *ACS Appl. Energy Mater.* 1 (2018) 3603–3606, <https://doi.org/10.1021/acsaem.8b00889>.
- [29] O. Sqalli, A. Oulmekki, M. Ijjaali, B. Malaman, M. Laaouini, Synthesis, crystal structure and magnetic properties of  $\text{Fe}_2\text{Pb}_{3-x}\text{Ba}_x(\text{PO}_4)_4$  ( $0 \leq x < 3$ ), *Mater. Lett.* 59 (2005) 1329–1333, <https://doi.org/10.1016/j.matlet.2005.01.005>.
- [30] R. Masse, A. Durif, Structure of tribarium dibismuth tetrakis(phosphate), *Acta Crystallogr. Sect. C*. 41 (1985) 1717–1718, <https://doi.org/10.1107/S0108270185009180>.
- [31] M. Hidouri, B. Lajmi, A. Wattiaux, L. Fournes, J. Darriet, M. Ben Amara, Crystal structure, magnetic properties and Mossbauer spectroscopy of  $\text{NaCaFe}_3(\text{PO}_4)_4$ , 358 (2003) 36–41, [https://doi.org/10.1016/S0925-8388\(03\)00129-4](https://doi.org/10.1016/S0925-8388(03)00129-4).
- [32] G.M. Sheldrick, SADABS version 2004/1, A Program for Empirical Absorption Correction, University of Göttingen, Göttingen, Germany, 2004.
- [33] G.M. Sheldrick, SHELXT - Integrated space-group and crystal-structure determination, *Acta Crystallogr. Sect. A Found. Adv.* 71 (2015) 3–8, <https://doi.org/10.1107/S2053273314026370>.
- [34] G.M. Sheldrick, Crystal structure refinement with SHELXL, *Acta Crystallogr. Sect. C Struct. Chem.* 71 (2015) 3–8. <https://doi.org/10.1107/S2053229614024218>.
- [35] L.J. Farrugia, WinGX and ORTEP for Windows: an update, *J. Appl. Crystallogr.* 45 (2012) 849–854. <https://doi.org/10.1107/S0021889812029111>.
- [36] H. Putz, K. Brandenburg, DIAMOND-Crystal and molecular structure visualization. Crystal Impact-GbR, Kreuzherrenstr, 102 (2006) 53227.
- [37] V. Petříček, M. Dušek, L. Palatinus, Crystallographic computing system JANA2006: General features, *Zeitschrift Fur Krist.* 229 (2014) 345–352, <https://doi.org/10.1515/zkri-2014-1737>.
- [38] A. Le Bail, Whole powder pattern decomposition methods and applications: A retrospection, *Powder Diffr.* 20 (2005) 316–326, <https://doi.org/10.1154/1.2135315>.
- [39] M. Whangbo, Ñ.H. Koo, D. Dai, Spin exchange interactions and magnetic structures of extended magnetic solids with localized spins : theoretical descriptions on formal , quantitative and qualitative levels, *J. Solid State Chem.* 176 (2003) 417–481, [doi:10.1016/S0022-4596\(03\)00273-1](https://doi.org/10.1016/S0022-4596(03)00273-1).
- [40] B.C. Melot, G. Rousse, J.N. Chotard, M. Ati, R.-C. J., M.C. Kemei, J.M. Tarascon, Magnetic Structure and Properties of the Li-Ion Battery Materials  $\text{FeSO}_4\text{F}$  and  $\text{LiFeSO}_4\text{F}$ , *Chem. Mater.* 23 (2011) 2922–2930, [doi:doi.org/10.1021/cm200465u](https://doi.org/10.1021/cm200465u).

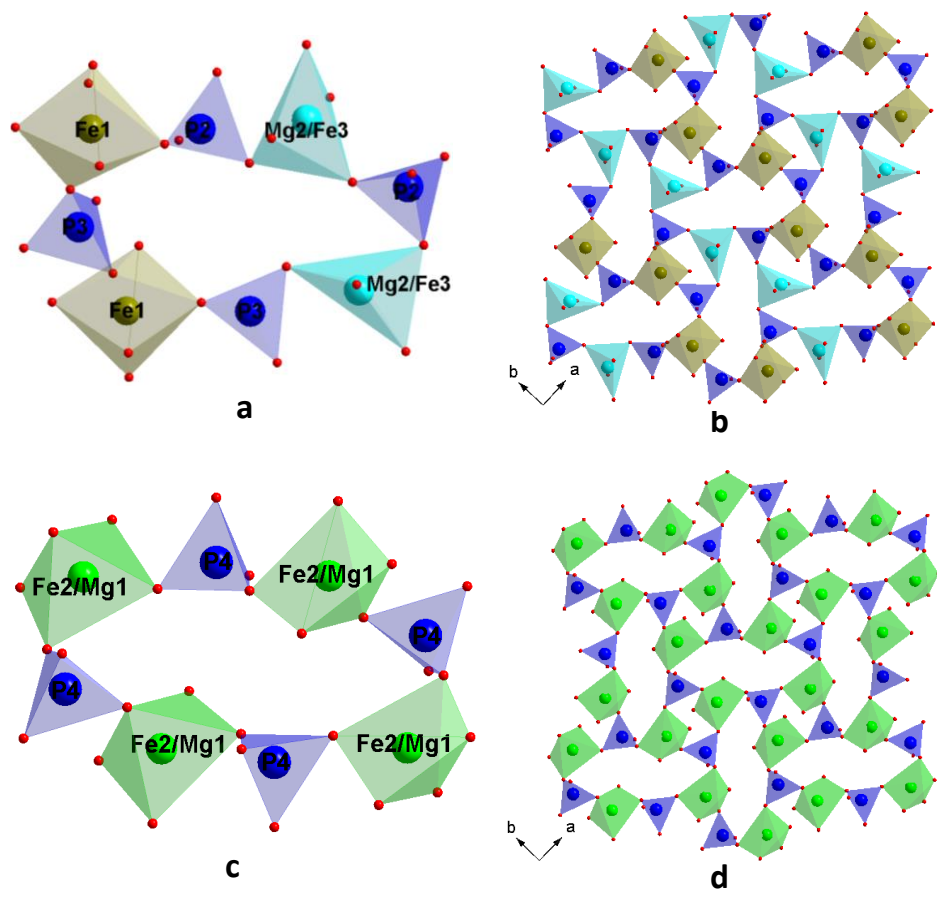


**Fig. 1:** **a)** First kind of ring with eight polyhedra. **b)** First type of sheet. **c)** Second kind of ring with eight polyhedra; **d)** Second type of sheet

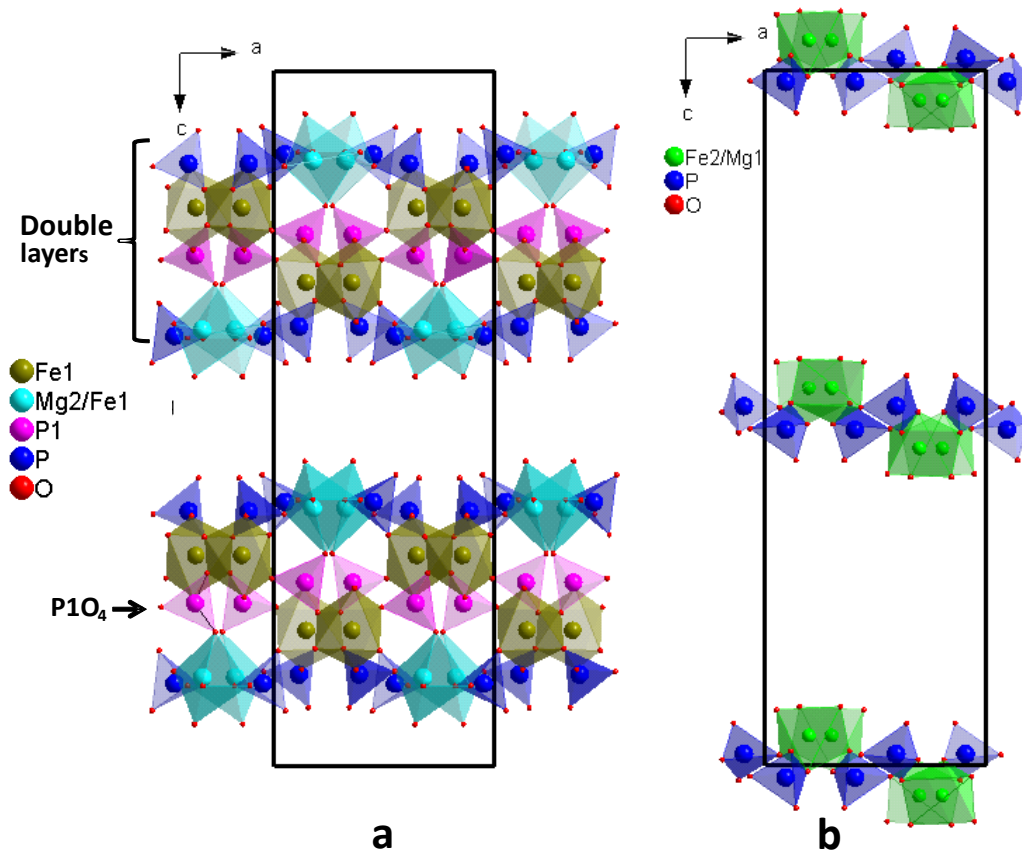


**Fig. 2:** a) Double layers resulting from two consecutive first kind rings connected together by  $P1O_4$  tetrahedra. b) Second type of sheet formed by the second kind rings

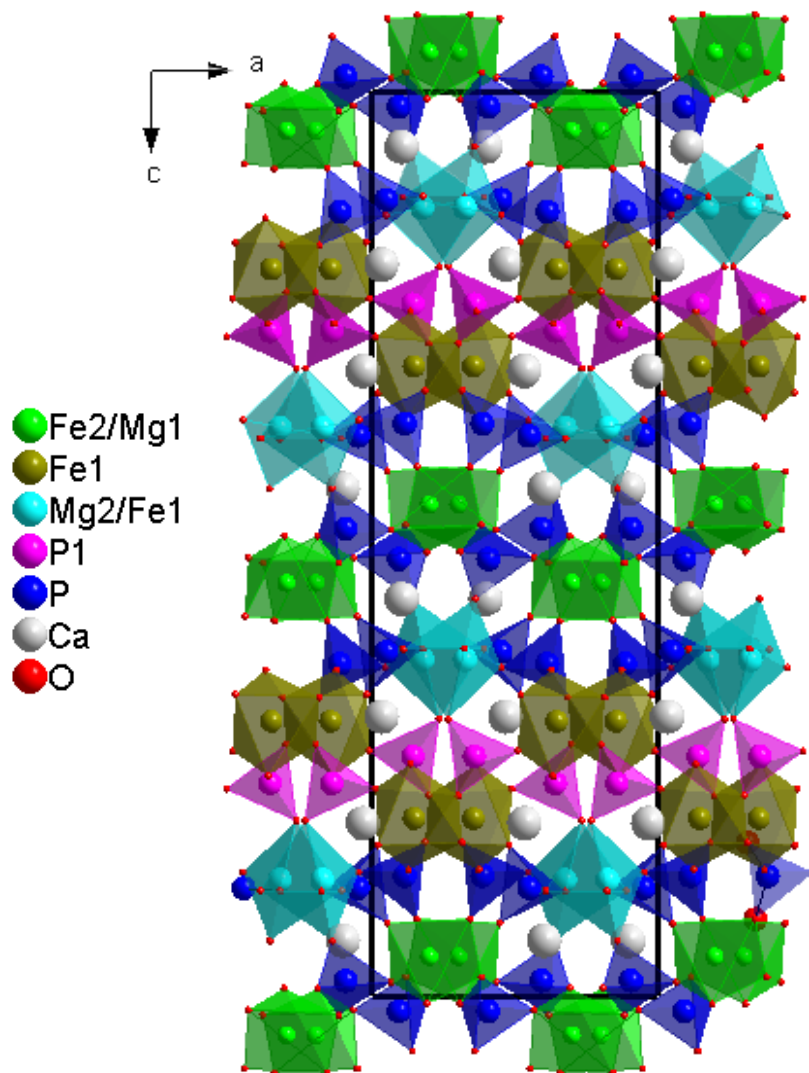


**Fig. 3:** Projection along  $[010]$  of  $\text{Ca}_2\text{MgFe}_2(\text{PO}_4)_4$  structure showing cavities occupied by  $\text{Ca}^{2+}$  cations

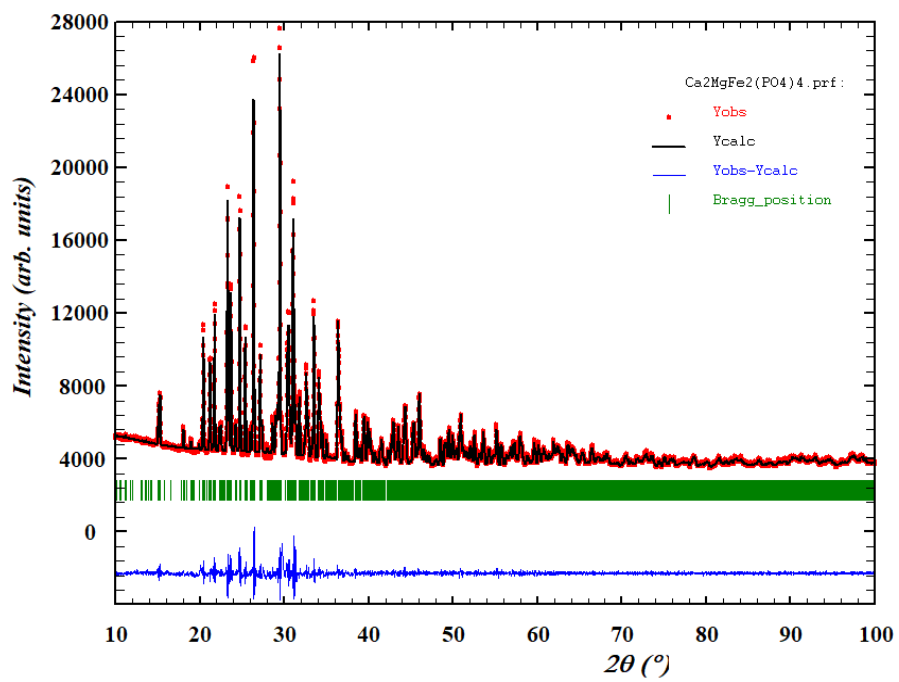


**Fig. 4:** The observed (black), calculated (red), difference (blue) and Bragg positions (green) for powder X-ray diffraction patterns of  $\text{Ca}_2\text{MgFe}_2(\text{PO}_4)_4$

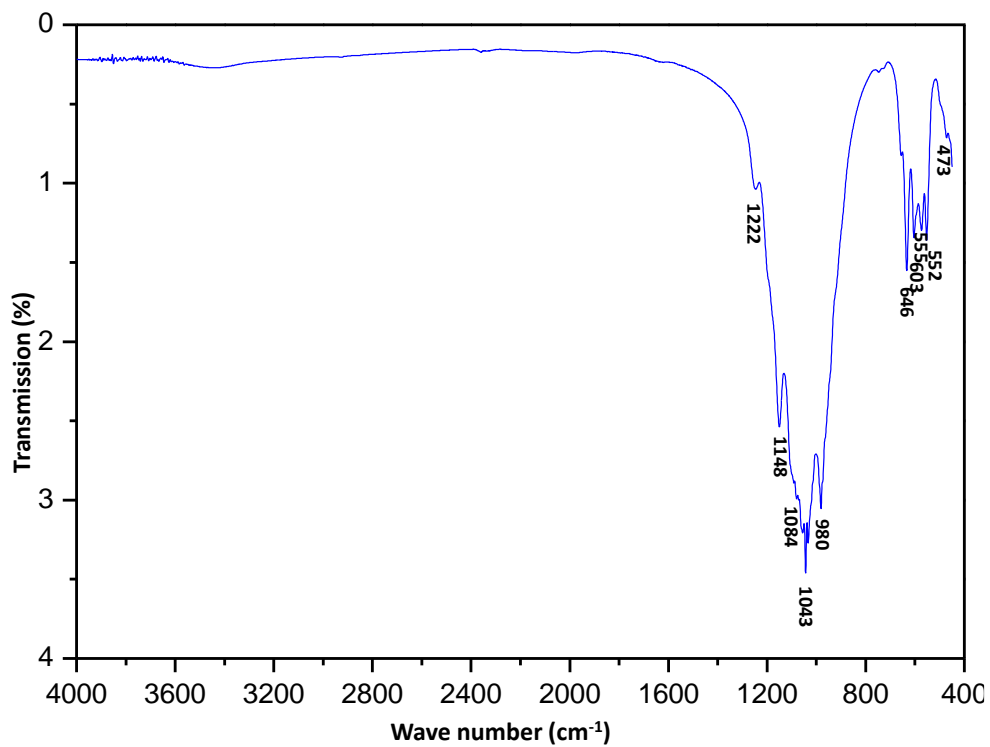


**Fig. 5:** Infrared spectrum of  $\text{Ca}_2\text{MgFe}_2(\text{PO}_4)_4$  powder.

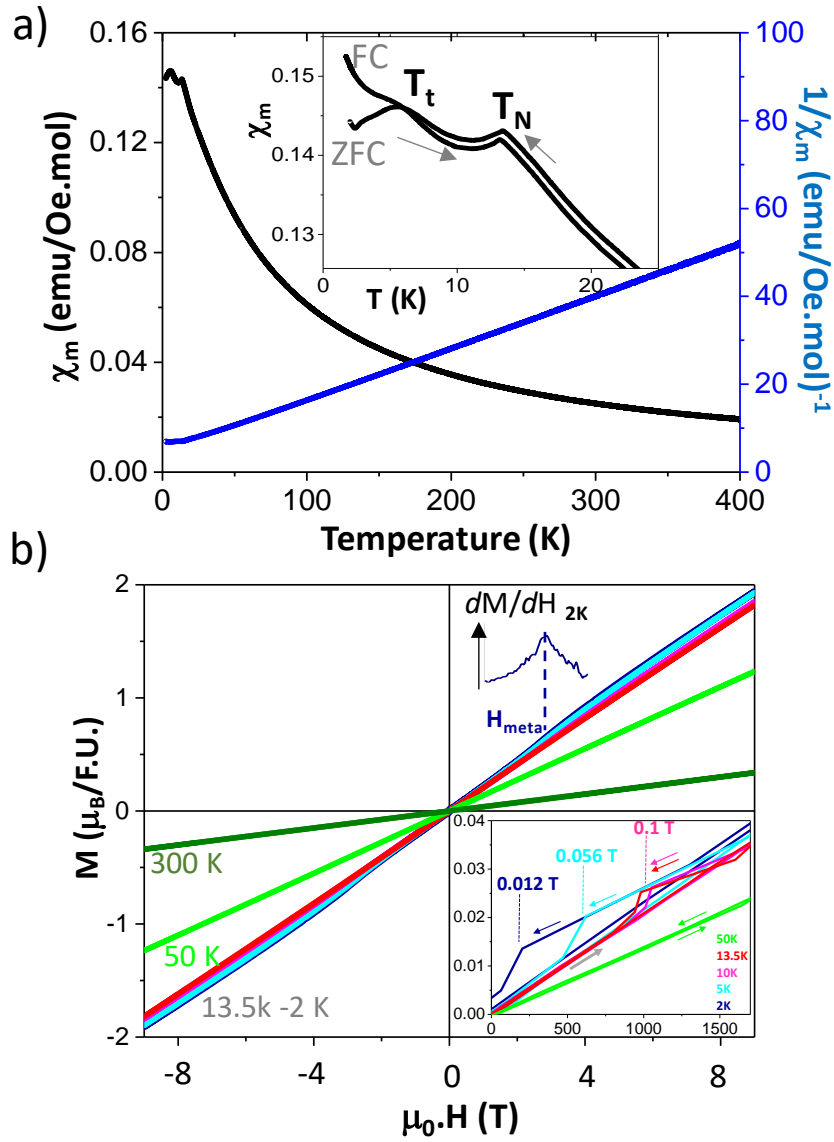


**Fig. 6:** a)  $\chi(T)$  and  $\chi^{-1}(T)$  for  $\text{Ca}_2\text{MgFe}_2(\text{PO}_4)_4$ . The inset shows the two transitions at  $T_N$  and  $T_t$  with ZFC/FC divergence below  $T_t$ . b) Magnetization versus field plots at various temperatures with a metamagnetic transition centered around 2.5 T at 2 K. The inset shows the critical field retaining the field-excited state below  $T_N$ .

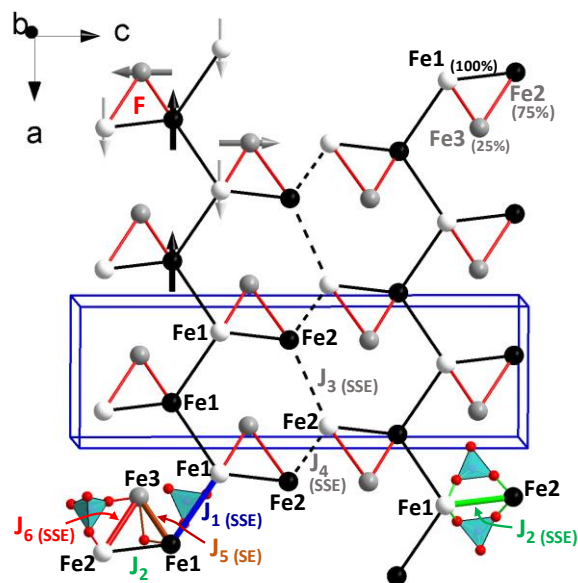


**Fig. 7:** Set of magnetic exchanges within the (a,b) layers. Black and white atoms represent spin up and spin down according to J1 to J4 exchanges. J5 and J6 add to Fe3 spins a frustrated topology (and compromised orientation) responsible for the metamagnetic transition.

**Table 1**

Crystal data and structure refinement for  $\text{Ca}_2\text{MgFe}_2(\text{PO}_4)_4$

<b>Crystal data</b>	
Chemical formula	$\text{Ca}_2\text{MgFe}_2(\text{PO}_4)_4$
Crystal system	Orthorhombique
Space group	Pbca
Cell dimension ( $\text{\AA}$ )	a = 9.3357 (7) b = 8.7340 (6) c = 29.422 (2)
Cell volume ( $\text{\AA}^3$ )	2399.0 (3)
Multiplicité Z	8
Molecular weight (g/mol)	596.05
Density ( $\text{g/cm}^{-3}$ )	3.301
Coefficient absorption $\mu$ ( $\text{mm}^{-1}$ )	3.96
<b>Data collection</b>	
Diffractometer	4-cercle Brüker X8 APEX- CCD
No. of measured, independent and observed [ $I \geq 2\sigma(I)$ ] reflections	20131, 3362, 3043
$R_{\text{int}}$	0.027
$\theta_{\text{max}}$ , $\theta_{\text{min}}$ ( $^\circ$ )	29.6 – 2.6
<b>Refinement</b>	
$R[F^2 > 2\sigma(F^2)]$	0.019
$wR(F^2)$	0.048
S (Goodness-of-Fit) :	1.08
No of refined parameters	226
$\Delta\rho_{\text{max}}$ , $\Delta\rho_{\text{min}}$ ( $\text{e}, \text{\AA}^{-3}$ )	0.55, -0.39

**Table 2:**Atomic coordinates, occupancies and equivalent isotropic displacement parameters ( $\text{\AA}^2$ ) for  $\text{Ca}_2\text{MgFe}_2(\text{PO}_4)_4$ 

Atom	Occupation	x	y	z	U <sub>eq</sub>
Fe1	1	0.64595 (3)	0.60846 (3)	0.196251 (8)	0.00527 (6)
Fe2/Mg1	0.75/0.25	0.69856 (3)	0.54472 (3)	0.043350 (9)	0.00511 (6)
Mg2/Fe3	0.75/0.25	0.32487 (5)	0.77518 (6)	0.12837 (1)	0.0105 (1)
P1	1	0.35795 (5)	0.81205 (5)	0.23506 (1)	0.00462 (8)
P2	1	0.45056 (5)	0.44136 (5)	0.11940 (1)	0.00579 (9)
P3	1	0.88616 (5)	0.41175 (5)	0.13281 (1)	0.00555 (8)
P4	1	0.40656 (5)	0.73416 (5)	0.01686 (1)	0.00601 (9)
Ca1	1	1.03281 (4)	0.66505 (4)	0.19113 (1)	0.00787 (7)
Ca2	1	0.39729 (4)	1.08148 (5)	0.06107 (1)	0.01321 (8)
O1	1	0.2661 (2)	0.7733 (2)	0.19375 (4)	0.0094 (2)
O2	1	0.3659 (1)	0.9861 (1)	0.24327 (4)	0.0082 (2)
O3	1	0.3019 (1)	0.7360 (1)	0.27836 (4)	0.0078 (2)
O4	1	0.5108 (1)	0.7488 (2)	0.22902 (4)	0.0095 (2)
O5	1	0.5201 (2)	0.4530 (2)	0.16660 (4)	0.0101 (3)
O6	1	0.5531 (2)	0.4634 (2)	0.08035 (5)	0.0163 (3)
O7	1	0.3915 (2)	0.2750 (1)	0.11648 (4)	0.0096 (2)
O8	1	0.3227 (2)	0.5504 (2)	0.11595 (4)	0.0131 (3)
O9	1	1.0475 (1)	0.4555 (2)	0.13681 (4)	0.0114 (3)
O10	1	0.8150 (1)	0.5065 (2)	0.16978 (4)	0.0106 (3)
O11	1	0.8736 (2)	0.2393 (2)	0.13965 (4)	0.0176 (3)
O12	1	0.8425 (2)	0.4595 (2)	0.08498 (4)	0.0154 (3)
O13	1	0.3592 (2)	0.8103 (2)	0.06101 (4)	0.0120 (3)
O14	1	0.5663 (2)	0.6958 (2)	0.01539 (5)	0.0127 (3)
O15	1	0.3826 (2)	0.8546 (2)	-0.02110 (4)	0.0127 (3)
O16	1	0.3081 (1)	0.5947 (1)	0.00867 (4)	0.0095 (2)

**Table 3**Anisotropic displacement parameters ( $\text{\AA}^2$ ) for  $\text{Ca}_2\text{MgFe}_2(\text{PO}_4)_4$ 

Atom	$U^{11}$	$U^{22}$	$U^{33}$	$U^{12}$	$U^{13}$	$U^{23}$
Fe1	0.0057 (1)	0.0050 (1)	0.0051 (1)	-0.00013 (9)	-0.00009 (8)	-0.00064 (8)
Fe2/Mg1	0.0050 (1)	0.0058 (1)	0.0046 (1)	-0.0001 (1)	-0.0001 (1)	0.00068 (9)
Mg2/Fe3	0.0135 (2)	0.0113 (2)	0.0067 (2)	-0.0051 (2)	0.0016 (2)	-0.0025 (2)
P1	0.0053 (2)	0.0040 (2)	0.0045 (2)	0.0001 (2)	0.0003 (1)	0.0000 (1)
P2	0.0059 (2)	0.0059 (2)	0.0055 (2)	-0.0014 (2)	0.0001 (2)	0.0006 (1)
P3	0.0069 (2)	0.0048 (2)	0.0050 (2)	0.0010 (2)	0.0004 (2)	0.0005 (1)
P4	0.0068 (2)	0.0049 (2)	0.0063 (2)	0.0006 (2)	0.0005 (2)	0.0002 (1)
Ca1	0.0083 (2)	0.0084 (2)	0.0069 (1)	-0.0002 (1)	0.0005 (1)	-0.0003 (1)
Ca2	0.0144 (2)	0.0131 (2)	0.0121 (2)	-0.0029 (2)	0.0006 (14)	-0.0038 (1)
O1	0.0102 (6)	0.0125 (6)	0.0055 (5)	-0.0025 (5)	-0.0016 (4)	-0.0008 (4)
O2	0.0133 (6)	0.0041 (5)	0.0072 (5)	-0.0002 (5)	0.0010 (5)	-0.0001 (4)
O3	0.0079 (6)	0.0085 (6)	0.0070 (5)	-0.0013 (5)	0.0007 (4)	0.0029 (4)
O4	0.0075 (6)	0.0104 (6)	0.0107 (5)	0.0028 (5)	0.0022 (5)	-0.0003 (5)
O5	0.0118 (6)	0.0101 (6)	0.0082 (5)	-0.0036 (5)	-0.0036 (5)	0.0002 (4)
O6	0.0153 (7)	0.0215 (8)	0.0121 (6)	-0.0055 (6)	0.0075 (5)	-0.0002 (5)
O7	0.0130 (7)	0.0073 (6)	0.0087 (5)	-0.0030 (5)	-0.0001 (5)	-0.0005 (4)
O8	0.0113 (7)	0.0137 (6)	0.0145 (6)	0.0045 (5)	-0.0019 (5)	-0.0013 (5)
O9	0.0069 (6)	0.0144 (7)	0.0128 (6)	0.0012 (5)	0.0011 (5)	-0.0045 (5)
O10	0.0102 (6)	0.0101 (6)	0.0115 (6)	0.0017 (5)	0.0036 (5)	-0.0035 (5)
O11	0.0379 (9)	0.0058 (6)	0.0091 (6)	0.0003 (6)	0.0045 (6)	0.0007 (5)
O12	0.0184 (7)	0.0192 (7)	0.0086 (6)	0.0057 (6)	-0.0025 (5)	0.0032 (5)
O13	0.0162 (7)	0.0110 (6)	0.0087 (6)	-0.0001 (5)	0.0029 (5)	-0.0023 (5)
O14	0.0072 (6)	0.0107 (6)	0.0200 (6)	0.0007 (5)	0.0004 (5)	-0.0008 (5)
O15	0.0122 (7)	0.0115 (6)	0.0143 (6)	0.0027 (5)	0.0030 (5)	0.0065 (5)
O16	0.0095 (6)	0.0081 (6)	0.0110 (6)	-0.0011 (5)	0.0000 (5)	-0.0007 (5)

**Table 4**The bond lengths (Å) for crystal  $\text{Ca}_2\text{MgFe}_2(\text{PO}_4)_4$ 

P1—O1	1.526 (1)	P3—O10	1.520 (1)
P1—O3	1.528 (1)	P3—O12	1.523 (1)
P1—O4	1.540 (1)	P3—O11	1.524 (1)
P1—O2	1.541 (1)	P3—O9	1.558 (1)
P2—O6	1.507 (1)	P4—O13	1.525 (1)
P2—O8	1.530 (1)	P4—O14	1.529 (1)
P2—O5	1.536 (1)	P4—O16	1.545 (1)
P2—O7	1.557 (1)	P4—O15	1.550 (1)
Fe1—O10	1.972 (1)	Fe2/Mg1—O6	1.880 (1)
Fe1—O3 <sup>iii</sup>	1.980 (1)	Fe2/Mg1—O16 <sup>i</sup>	1.957 (1)
Fe1—O5	1.996 (1)	Fe2/Mg1—O12	1.965 (1)
Fe1—O4	2.006 (1)	Fe2/Mg1—O14	1.986 (1)
Fe1—O11 <sup>iv</sup>	2.028 (1)	Fe2/Mg1—O15 <sup>ii</sup>	2.038 (1)
Fe1—O2 <sup>v</sup>	2.079 (1)		
Mg2/Fe3—O9 <sup>iv</sup>	1.991 (1)	Mg2/Fe3—O13	2.031 (1)
Mg2/Fe3—O8	1.997 (2)	Mg2/Fe3—O7 <sup>vi</sup>	2.050 (2)
Mg2/Fe3—O1	2.001 (1)	<Mg2/Fe3—O>	2.014
Ca1—O1 <sup>vii</sup>	2.375 (1)	Ca2—O7 <sup>ix</sup>	2.349 (1)
Ca1—O2 <sup>viii</sup>	2.385 (1)	Ca2—O13	2.395 (1)
Ca1—O3 <sup>iii</sup>	2.416 (1)	Ca2—O15 <sup>x</sup>	2.433 (1)
Ca1—O9	2.433 (1)	Ca2—O16 <sup>vi</sup>	2.463 (1)
Ca1—O4 <sup>iii</sup>	2.469 (1)	Ca2—O9 <sup>iv</sup>	2.538 (1)
Ca1—O7 <sup>iv</sup>	2.499 (1)	Ca2—O8 <sup>vi</sup>	2.627 (1)
Ca1—O10	2.539 (1)	Ca2—O12 <sup>iv</sup>	2.744 (2)
Ca1—O5 <sup>iv</sup>	2.663 (1)	Ca2—O11	2.994 (1)

Symmetry codes : (i)  $-x+1, -y+1, -z$ ; (ii)  $x+1/2, -y+3/2, -z$ ; (iii)  $x+1/2, y, -z+1/2$ ; (iv)  $-x+3/2, y+1/2, z$ ; (v)  $-x+1, y-1/2, -z+1/2$ ; (vi)  $-x+1/2, y+1/2, z$ ; (vii)  $x+1, y, z$ ; (viii)  $-x+3/2, y-1/2, z$ ; (ix)  $x, y+1, z$ ; (x)  $-x+1, -y+2, -z$ .

**Table 5**

Geometry of the paths within the main in-plane magnetic exchanges and their estimated strengths

	Fe-Fe (Å)	Fe-O (Å)	O-Fe (Å)	O—O(Å)	∠ Fe-O-O-Fe (°)
<b>J1 (Fe1-O4-O3-Fe1)</b>	5.64	2.00	1.98	2.43	13.7 .... weak
<b>J2 (Fe1-O10-O12-Fe2)</b>	4.56	1.97	1.96	2.54	5.8 ..... strong
<b>(Fe1-O5-O6-Fe2)</b>	-	1.99	1.88	2.56	18.7
<b>J3 (Fe2-O16-O14-Fe2) 2x</b>	4.57	1.96	1.98	2.57	77.7 .....weak
<b>J4 (Fe1-O5-O8-Fe3)</b>	3.88	1.99	2.00	2.52	10.0 .... Strong
<b>(Fe1-O4-O1-Fe3)</b>	-	2.00	2.00	2.52	40.1
<b>(Fe1-O11-O9-Fe3)</b>	-	2.03	2.49	1.99	77.2
<b>J5 (Fe2-O14-O13-Fe3)</b>	4.74	1.98	2.03	2.56	6.2 .... medium
<b>(Fe2-O6-O8-Fe3)</b>	-	1.88	1.99	2.55	28.3